

Symmetry Breaking and Error Correction in Open Quantum Systems

Simon Lieu,^{1,2} Ron Belyansky,^{1,2} Jeremy T. Young,¹ Rex Lundgren,^{1,2} Victor V. Albert^{1b,2,3,4} and Alexey V. Gorshkov^{1b,2}

¹Joint Quantum Institute, NIST/University of Maryland, College Park, Maryland 20742, USA

²Joint Center for Quantum Information and Computer Science, NIST/University of Maryland, College Park, Maryland 20742, USA

³Institute for Quantum Information and Matter and Walter Burke Institute for Theoretical Physics, California Institute of Technology, Pasadena, California 91125, USA

⁴National Institute of Standards and Technology, Gaithersburg, Maryland 20899, USA



(Received 6 August 2020; accepted 10 November 2020; published 8 December 2020)

Symmetry-breaking transitions are a well-understood phenomenon of closed quantum systems in quantum optics, condensed matter, and high energy physics. However, symmetry breaking in open systems is less thoroughly understood, in part due to the richer steady-state and symmetry structure that such systems possess. For the prototypical open system—a Lindbladian—a unitary symmetry can be imposed in a “weak” or a “strong” way. We characterize the possible \mathbb{Z}_n symmetry-breaking transitions for both cases. In the case of \mathbb{Z}_2 , a weak-symmetry-broken phase guarantees at most a classical bit steady-state structure, while a strong-symmetry-broken phase admits a partially protected steady-state qubit. Viewing photonic cat qubits through the lens of strong-symmetry breaking, we show how to dynamically recover the logical information after any gap-preserving strong-symmetric error; such recovery becomes perfect exponentially quickly in the number of photons. Our study forges a connection between driven-dissipative phase transitions and error correction.

DOI: [10.1103/PhysRevLett.125.240405](https://doi.org/10.1103/PhysRevLett.125.240405)

While an open quantum system typically evolves toward a thermal state [1], nonthermal steady states emerge in the presence of an external drive [2,3] or via reservoir engineering [4,5]. In particular, systems with multiple steady states have recently attracted much attention due to their ability to remember initial conditions [6–18]. For Markovian environments, this involves studying Lindblad superoperators (Lindbladians) [19–21] that possess multiple eigenvalues of zero [22].

On the one hand, Lindbladians with such degenerate steady states are the key ingredient for *passive* error correction [23–34]. In this paradigm, the degenerate steady-state structure of an appropriately engineered Lindbladian stores the logical information, and the Lindbladian passively protects this information from certain errors by continuously mapping any leaked information back into the structure without distortion. An important task remains to identify *generic* systems that host such protected qubit steady-state structures, and classify the errors that can be corrected in this way.

On the other hand, the presence of a ground-state degeneracy in the infinite-size limit of a closed system is a salient feature of symmetry breaking (e.g., the ferromagnetic ground states of the Ising model) [35]. While the study of analogous phase transitions in open systems has become a rich and active field [3,36–49] with significant experimental relevance [50–54], attention has focused on the steady-state degeneracy in symmetry-broken phases only recently [55–57].

Since steady-state degeneracy is a requirement for both passive error correction and symmetry breaking, it is natural to ask whether there are any connections between the two phenomena. Here, we begin to shed light on this interesting and important direction by (A) describing how the dimension and structure of the steady-state manifold changes across a dissipative phase transition, and (B) identifying any passive protection due to the symmetry-broken phase (we will often drop the word symmetry below).

To this end, we emphasize an important distinction between “weak” and “strong” transitions which is unique to open systems. This difference stems from the dissipative part of the Lindbladian which can respect a symmetry in two separate ways, as first noted by Buča and Prosen [6]. We show that the \mathbb{Z}_2 strong-broken phase encodes a qubit in its steady-state structure in the infinite-size limit, and that errors preserving this structure can be passively corrected. Our analysis is made concrete by considering a driven-dissipative photonic mode—a minimal model for the study of both nonequilibrium transitions [55] and bosonic error-correcting codes [25].

Generic \mathbb{Z}_n symmetry breaking.—We consider open systems governed by a Lindblad master equation

$$\frac{d\rho}{dt} = \mathcal{L}(\rho) = -i[H, \rho] + \sum_i (2L_i \rho L_i^\dagger - \{L_i^\dagger L_i, \rho\}), \quad (1)$$

with density matrix ρ , Hamiltonian H , dissipators L_i , and Lindbladian \mathcal{L} . A *strong* symmetry is satisfied if there

exists an operator P such that $[H, P] = [L_i, P] = 0$, $\forall i$. A *weak* symmetry is satisfied if $[\mathcal{L}, \mathcal{P}] = 0$, where $\mathcal{P}(\cdot) = P(\cdot)P^\dagger$. A strong symmetry necessarily implies a weak symmetry but the converse is not true. For example, the dissipators only need to commute up to a phase ($L_i P = e^{i\theta_i} P L_i$) for the weak condition to be met. We will showcase differences between previously studied weak-symmetry transitions and the strong-symmetry ones we introduce here, focusing on changes to the dimension *and* structure of the steady-state manifold.

Let us review [55] weak \mathbb{Z}_2 -symmetry breaking, which is similar to conventional closed-system symmetry breaking and is ubiquitous in open systems [36,45,46]. Here, P is a parity operator that satisfies $P|\pm\rangle = \pm|\pm\rangle$ with parity eigenvalues ± 1 and sets of eigenstates $\{|\pm\rangle\}$. Its superoperator version, $\mathcal{P}(\cdot) = P(\cdot)P^\dagger$, possesses $+1$ and -1 “superparity” eigenvalues, belonging respectively to eigenoperators $|\pm\rangle\langle\pm|$ and $|\pm\rangle\langle\mp|$. A weak \mathbb{Z}_2 symmetry \mathcal{P} can thus be used to block diagonalize \mathcal{L} into two sectors, $\mathcal{L} = \text{diag}[\mathcal{L}_+, \mathcal{L}_-]$, one for each superparity. Since the -1 superparity sector contains only traceless eigenoperators, the (trace-one) steady state of a finite-size system will necessarily have superparity $+1$ and be an eigenoperator of \mathcal{L}_+ . If a symmetry-broken order parameter is to acquire a nonzero steady-state expectation value in the infinite-size limit, \mathcal{L}_- must also pick up a zero-eigenvalue eigenoperator, and positive or negative mixtures of the original steady state and this new eigenoperator will become the two steady states of the system (a “1-to-2” transition).

In the strong case, there are two superparity superoperators, $\mathcal{P}_l(\cdot) = P(\cdot)$ and $\mathcal{P}_r(\cdot) = (\cdot)P^\dagger$, that commute with each other as well as with \mathcal{L} . Their eigenvalues further resolve the states $|+\rangle\langle+|$ from $|-\rangle\langle-|$ (and similarly $|+\rangle\langle-|$ from $|-\rangle\langle+|$), yielding the finer block diagonalization $\mathcal{L} = \text{diag}[\mathcal{L}_{++}, \mathcal{L}_{--}, \mathcal{L}_{+-}, \mathcal{L}_{-+}]$. The key observation is that both \mathcal{L}_{++} and \mathcal{L}_{--} have to admit steady-state eigenoperators, since their respective sectors house eigenoperators with nonzero trace. A strong transition is therefore a 2-to-4 transition: the dimension of the steady-state manifold increases from 2 to 4 as \mathcal{L}_{-+} and \mathcal{L}_{+-} pick up zero eigenvalues in the broken phase. This reasoning generalizes to \mathbb{Z}_n symmetries (see Table I).

Steady-state structure in different \mathbb{Z}_2 phases.—Apart from differences in the dimension of the steady-state manifold, a weak-broken \mathbb{Z}_2 phase can yield at most a

classical bit structure, while a strong-broken phase can yield a qubit steady-state manifold. To see this, we express the steady state of a \mathbb{Z}_2 -symmetric model in the parity basis, $|\vec{\pm}\rangle = (|\pm\rangle_1, |\pm\rangle_2, \dots)$, as

$$\rho_{ss} = \begin{pmatrix} s_{++} & s_{+-} \\ s_{-+} & s_{--} \end{pmatrix}. \quad (2)$$

Table II lists the “degrees of freedom” for the steady state in each phase, i.e., which part of the matrix is allowed to change depending on the initial condition ρ_i . The strong-broken phase can remember both the relative magnitude and phase of an initial state, which guarantees that a qubit can be encoded into the steady state. The strong-unbroken and weak-broken phases both host a classical bit structure, where classical mixtures remain stable. The weak-unbroken phase will generically possess a unique steady state.

\mathbb{Z}_2 -symmetric model.—We make this general analysis more concrete by focusing on a minimal driven-dissipative example that exhibits both strong and weak versions of \mathbb{Z}_2 symmetry-breaking transitions in an infinite-size limit. Consider the rotating-frame Hamiltonian for a photonic cavity mode subject to a coherent two-photon drive:

$$H = \omega a^\dagger a + \lambda[a^2 + (a^\dagger)^2], \quad (3)$$

where $\omega, \lambda \in \mathbb{R}$ [10,25,58–60]. The Hamiltonian possesses a \mathbb{Z}_2 symmetry with respect to Bose parity: $[H, P] = 0$, where $P = \exp(i\pi a^\dagger a)$. Dissipation can be introduced in ways that respect strong or weak versions of the parity symmetry. We present our strong case along with the previously studied weak case [55], further developing the latter.

In the strong case, we consider two-photon loss $L_2 = \sqrt{\kappa_2} a^2$ and dephasing $L_d = \sqrt{\kappa_d} a^\dagger a$. In the weak case, we add one-photon loss $L_1 = \sqrt{\kappa_1} a$ in addition to L_2 and L_d . Note that $[L_2, P] = [L_d, P] = 0$ and $\{L_1, P\} = 0$, which justifies our classification. The competition between non-commuting terms in the Hamiltonian results in a symmetry-broken phase for large ratios of λ/ω , as described below.

We uncover the phase diagram using two independent methods that agree: (1) a solution for the order parameter and (2) an expression for the dissipative gap. The expectation value of the order parameter a satisfies

TABLE I. Comparison of a strong vs weak \mathbb{Z}_n symmetry of \mathcal{L} . The final column describes transitions in the dimension of the steady state (D_{SS}) manifold (number of zero eigenvalues of \mathcal{L}) when going from the unbroken phase to the broken phase.

\mathbb{Z}_n symmetry	Definition	Sufficient condition	D_{SS} transition
Strong	$[\mathcal{L}, \mathcal{P}_{l,r}] = 0$	$[H, P] = [L_i, P] = 0$	n -to- n^2
Weak	$[\mathcal{L}, \mathcal{P}] = 0$	$[H, P] = \{L_i, P\} = 0$	1-to- n

TABLE II. The structure and participating degrees of freedom of the steady state (SS) matrix in Eq. (2) for different \mathbb{Z}_2 phases.

\mathbb{Z}_2 phase	SS freedom	SS structure
Strong, broken	$s_{++}, s_{--}, s_{+-}, s_{-+}$	Qubit
Strong, unbroken	s_{++}, s_{--}	Classical bit
Weak, broken	s_{+-}, s_{-+}	Classical bit
Weak, unbroken	None	Unique

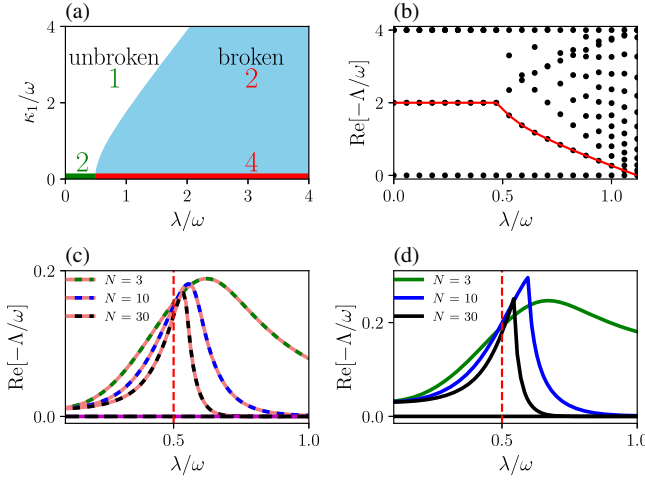


FIG. 1. (a) Phase diagram for the model in Eq. (3) with one-photon loss κ_1 , $\kappa_d = 0$, in the thermodynamic limit $\lambda/\kappa_2 \rightarrow \infty$. Integers indicate the dimension of the steady-state manifold. (b) Analytical expression for the dissipative gap (red line) and numerical spectrum (black dots) in the unbroken phase for $\kappa_2 = \kappa_d = 0$, $\kappa_1/\omega = 2$. The dissipative gap closes as the phase boundary at $\lambda/\omega = \sqrt{5}/2 \approx 1.1$ is approached. (c) Strong transition: decay rate of the four modes with the longest lifetime; two modes are always pinned to zero and the other two are degenerate (textured colors indicate twofold degeneracy of all modes in this subfigure). A 2-to-4 transition occurs near $\lambda/\omega = 0.5$ (red dashed line) in the limit $N \rightarrow \infty$, in agreement with the phase diagram. $\kappa_1 = 0$, $\lambda/\kappa_2 = N$, $\kappa_d/\omega = 0.01$. (d) Weak transition: decay rate of the two modes with the longest lifetime. Full lines emphasize a lack of exact twofold degeneracy present in (c). A 1-to-2 transition is observed. $\lambda/\kappa_2 = N$, $\kappa_1/\omega = 0.02$, $\kappa_d/\omega = 0.01$.

$$\frac{d}{dt} \langle a \rangle = -2i\lambda \langle a^\dagger \rangle - (i\omega + \kappa_1 + \kappa_d) \langle a \rangle - 2\kappa_2 \langle a^\dagger a^2 \rangle, \quad (4)$$

where the right-hand side follows from $\partial_t \langle a \rangle = \text{Tr}[a\mathcal{L}(\rho)]$. To determine the steady-state expectation value, we set $\partial_t \langle a \rangle_{ss} = 0$ and check which parameter regime produces nontrivial solutions for $\langle a \rangle_{ss} \equiv \alpha$. In the mean-field approximation, $\langle a^\dagger a^2 \rangle \approx |\alpha|^2 \alpha$, which is justified when $|\alpha|^2$ (the cavity photon population) is large. The critical boundary satisfies $(\kappa_1 + \kappa_d)/\omega = \sqrt{4(\lambda/\omega)^2 - 1}$, with a cavity photon population $|\alpha|^2 = [\sqrt{4\lambda^2 - \omega^2} - (\kappa_1 + \kappa_d)]/(2\kappa_2)$ and $\arg[\alpha] = \arccos[-\omega/(2\lambda)]/2$ in the broken phase. The steady-state population of photons diverges as $\lambda/\kappa_2 \equiv N \rightarrow \infty$, which represents the thermodynamic limit for this model [55,57,61,62]. Figure 1(a) presents the phase diagram for $\lambda/\kappa_2 \rightarrow \infty$; the mean-field equation is exact in this limit. Both weak ($\kappa_1 \neq 0$) and strong ($\kappa_1 = 0$) models indeed exhibit a transition characterized by a \mathbb{Z}_2 -broken order parameter $\langle a \rangle_{ss}$.

We show that the dissipative gap closes at the critical boundary for $\kappa_2 = \kappa_d = 0$. In this (thermodynamic) limit, \mathcal{L} is quadratic in Bose operators, hence we can calculate the dissipative gap in the unbroken phase:

$\Delta_g = -\text{Re}[\kappa_1 + \sqrt{4\lambda^2 - \omega^2}]$ [see Supplemental Material (SM) [63]]. Setting $\Delta_g = 0$ leads to a phase boundary which is identical to the mean-field analysis plotted in Fig. 1(a). Figure 1(b) plots the expression for Δ_g along with a numerical calculation of the Lindblad spectrum $\{\Lambda\}$, defined via $\mathcal{L}(e_j) = \Lambda_j e_j$ where e_j are eigenoperators of \mathcal{L} with eigenvalues Λ_j . We expect an extensive number of modes to touch zero at the critical point $\lambda \approx 1.1$, but our numerics are limited by a finite Hilbert space. Similar results were recently reported in a related model [67].

Away from this exactly solvable limit, i.e., $\kappa_2 \neq 0$ and/or $\kappa_d \neq 0$, we use numerical exact diagonalization to examine the steady-state dimension across the boundary. Figure 1(c) probes the strong transition by plotting the four spectral eigenvalues with the smallest decay rate. Indeed, two of these are always pinned to zero due to the strong symmetry, but two additional zero eigenvalues appear in the broken phase. The transition occurs near values predicted by the phase diagram as the system approaches the thermodynamic limit $\lambda/\kappa_2 = N \rightarrow \infty$. We repeat the analysis for the weak transition in Fig. 1(d) by plotting the two modes with the longest lifetimes and observe a 1-to-2 transition. This confirms our general analysis in Table I. The degeneracy at zero in the broken phase is split by an exponentially small term $\sim \exp(-N)$ (see SM [63]).

The rest of our analysis will focus on the strongly symmetric model, setting $\kappa_1 = 0$. We inspect the nature of the steady states by writing down their exact expressions in extreme limits. First consider the unbroken phase $\omega \neq 0$, $\kappa_2 \neq 0$, $\lambda = \kappa_d = 0$. There are only two eigenoperators of \mathcal{L} with zero eigenvalue $|0\rangle\langle 0|$ and $|1\rangle\langle 1|$. The steady-state manifold reads $\rho_{ss}(x) = x|0\rangle\langle 0| + (1-x)|1\rangle\langle 1|$ for $x \in [0, 1]$. This represents a classical bit of information, since only relative magnitudes of an initial superposition are remembered, in agreement with Table II.

Next, consider the broken limit $\omega = \kappa_d = 0$, $\lambda \neq 0$, $\kappa_2 \neq 0$. Define the following coherent states $|\pm\alpha\rangle = \sum_{n=0}^{\infty} (\pm\alpha)^n |n\rangle / \sqrt{n!}$ where $\pm\alpha = \pm e^{i\pi/4} \sqrt{\lambda/\kappa_2}$. α matches the mean-field result, defined up to a minus sign degeneracy. Then any pure state of the form $|\psi\rangle = c_e |\alpha\rangle_e + c_o |\alpha\rangle_o$ will be a steady state, where we define normalized even and odd “cat” coherent states $|\alpha\rangle_{e,o} \propto |\alpha\rangle \pm |-\alpha\rangle$ [68]. An arbitrary superposition of these cat states is a steady state, an example of a decoherence-free subspace (DFS) [23].

Passive error correction for cat qubits.—We now show that a qubit encoded in the steady-state subspace of the strong-broken phase benefits from passive error correction in the thermodynamic limit $\lambda/\kappa_2 = N \rightarrow \infty$. We have just seen that the limit $\kappa_1 = \kappa_d = \omega = 0$ hosts a DFS spanned by cat states. We define \mathcal{L}_0 to be the Lindbladian at this point. Previous studies have suggested that this coherent subspace could serve as a platform for universal quantum computation that is intrinsically protected against dephasing errors [25]. Reference [25] found that, as $|\alpha|^2 \rightarrow \infty$, an

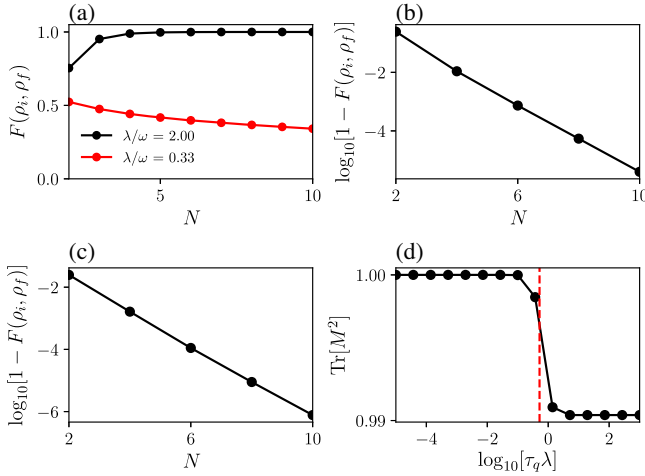


FIG. 2. (a) Fidelity of the initial and final states for the quench protocol given in the main text with $\lambda/\kappa_2 = N$, $\kappa_d = 0$, $\tau_q \lambda = 10$, $F(\rho_i, \rho_f) = \text{Tr}[\sqrt{\sqrt{\rho_i} \rho_f \sqrt{\rho_i}}]$. Quenches to the strong-broken phase (black dots) have a fidelity that tends to one in the thermodynamic limit, while quenches to the strong-unbroken phase (red dots) do not. (b) Same parameters as in (a) with $\lambda/\omega = 2$; the fidelity tends to one exponentially fast in N . (c) A dephasing error $\kappa_d/\lambda = 0.03$, $\omega = 0$, $\lambda/\kappa_2 = N$, $\tau_q \lambda = 10$; again the fidelity is exponentially close to one. (d) Purity of M [see Eq. (5)] for different quench times with the same parameters as in (b) and $N = 15$. The dashed line is the timescale set by the dissipative gap $\tau_g = \Delta_g^{-1}$ of $\mathcal{L}_0 + \mathcal{L}'$. (Δ_g is the decay rate of the longest-lived excitation above the four steady-state solutions.) Short quenches keep the system approximately pure, while long quenches evolve the system to a mixed NS steady state. Errors are correctable in both cases. For all figures, $c_e = 1/\sqrt{2}$, $c_o = i/\sqrt{2}$.

initially pure cat qubit, which encounters a dephasing term in the Lindbladian for a short time (with respect to the inverse dissipative gap) will return to its initial pure state after evolving the system with \mathcal{L}_0 . In this context, our analysis allows us to (1) extend the protection to errors that last an *arbitrary* amount of time (cf. [69]), (2) understand the dynamics of the state throughout the error process, and (3) classify the types of errors that self correct via the environment.

We consider the following protocol: Initialize the system in a pure state $\rho_i = |\psi\rangle\langle\psi|$, $|\psi\rangle = c_e|\alpha\rangle_e + c_o|\alpha\rangle_o$, which represents the qubit and satisfies $\mathcal{L}_0(\rho_i) = 0$. Then quench the state with an “error” for an arbitrary time τ_q to obtain $\rho_m = \exp[(\mathcal{L}_0 + \mathcal{L}')\tau_q](\rho_i)$. Finally, turn off the error and evolve the system with \mathcal{L}_0 for a long time such that it reaches its steady state: $\rho_f = \lim_{t \rightarrow \infty} \exp[\mathcal{L}_0 t](\rho_m)$. For what types of perturbations \mathcal{L}' will ρ_f and ρ_i be equal?

In Figs. 2(a) and 2(b), we plot the fidelity F between the initial state and the final state for the protocol described above with an error in the frequency, i.e., $H' = \omega a^\dagger a$, which either keeps the system in the strong-broken phase (black dots) or moves it to the strong-unbroken phase (red dots). The fidelity tends to one exponentially fast in cavity photon

number for a long quench time τ_q *only* if the perturbation kept the system in the broken phase. Figure 2(c) shows a similar behavior in the presence of a dephasing error: The qubit is able to perfectly correct itself as $N \rightarrow \infty$.

We can understand this striking behavior by recalling that the system is guaranteed to host a qubit steady state structure in the $N \rightarrow \infty$ limit of the strong-broken phase. Away from the special point \mathcal{L}_0 but within the strong-broken phase, our numerics suggest that the steady-state structure is a noiseless subsystem (NS) [70]: a qubit in any state tensored with a fixed mixed state. In other words, at any time after the introduction of the error, the state has the form

$$\rho_m(\tau_q) = \begin{pmatrix} |c_e|^2 & c_e c_o^* \\ c_e^* c_o & |c_o|^2 \end{pmatrix} \otimes M(\tau_q), \quad (5)$$

where the qubit factor remains perfectly encoded in the even-odd parity basis, while the state $M(\tau_q)$ interpolates between the (pure) DFS steady state and the (mixed) NS steady state. The purity of $M(\tau_q)$ for different quench times is given in Fig. 2(d), corroborating this interpretation: Short quenches leave M approximately pure, while long quenches allow it to equilibrate to a mixed steady state (cf. [34]). In both cases, the initial qubit state can be restored via evolution by \mathcal{L}_0 , with most of the recovery (up to exponentially small corrections) occurring after a time of order of the inverse dissipative gap. This decoupling of the qubit from auxiliary modes is reminiscent of the decoupling used in quantum-information-preserving sympathetic cooling of trapped ions [71] and neutral atoms [72], as well as in the nuclear-spin-preserving manipulation of electrons in alkaline-earth atoms [73,74]. The SM [63] provides numerical evidence for the structure in Eq. (5), including the NS steady state of $\mathcal{L}_0 + \mathcal{L}'$. The SM [63] also shows perfect recovery of the fidelity for long quenches via an independent method, i.e., asymptotic projections [8].

The argument above relies on the presence of a qubit steady-state structure for $\mathcal{L}_0 + \mathcal{L}'$ in the large- N limit. In its absence, the error will immediately cause the state to lose information about the relative magnitude and/or phase of c_e, c_o , which define the qubit. We conjecture that any error \mathcal{L}' which keeps the model in the strong-broken phase can

TABLE III. Examples of errors that can and cannot be passively corrected via evolution by \mathcal{L}_0 for the protocol given in the main text. An error must preserve the strong symmetry *and* keep the model in the broken phase in order for the final state to match the initial one.

Error	Strong?	Broken?	Correcting?
$L_1 = \sqrt{\kappa_1} a, \lambda/\kappa_1 > 0.5$	No	Yes	No
$H' = \omega a^\dagger a, \lambda/\omega < 0.5$	Yes	No	No
$H' = \omega a^\dagger a, \lambda/\omega > 0.5$	Yes	Yes	Yes
$L'_d = \sqrt{\kappa_d} a^\dagger a, \lambda/\kappa_d > 0.5$	Yes	Yes	Yes

be passively corrected, which agrees with Fig. 2(a). Table III provides a list of potential errors. Our framework allows us to classify the terms that are expected to self correct via \mathcal{L}_0 . Analytical proof of this conjecture requires an exact solution for the steady states in the entire strong-broken phase—an open direction for future work.

Discussion and outlook.—Recent experiments have made progress on the stabilization and manipulation of photonic cat qubits encoded into superconducting resonators [58,75–80]. Our study shows that certain errors which arise via coherent Hamiltonian terms can be passively corrected. For example, Ref. [81] proposes that $H = \omega a^\dagger a$ processes are useful for parity checks, Toffoli gates, and X gates. If this term unintentionally acts on some other qubit, then an error occurs. Such errors get passively corrected via \mathcal{L}_0 once the manipulation ends. Further, our analysis shows that logical information can be stored in the steady state even in the presence of terms which are beyond experimental control, e.g., $\kappa_d \neq 0$.

Although single-photon loss can induce qubit errors which are not correctable passively (the dominant decoherence mechanism in experiments), in the SM [63] we show that a *classical* bit encoded in \mathcal{L}_0 will recover from errors which keep $\mathcal{L}_0 + \mathcal{L}'$ in the *weak-broken* phase. Our setup thus admits a tunable classical-quantum steady-state structure. For qubits, this implies that modest single-photon loss induces passively correctable bit-flip errors, as well as phase-flip errors that require active correction.

While we have studied a \mathbb{Z}_2 -symmetric system, a \mathbb{Z}_n -symmetric model should host a similarly protected qubit in the strong-broken phase. Our symmetry-breaking analysis should also apply to examples in Dicke-model physics [36], multimode systems [82], molecular platforms [83], and trapped ions [4,84].

In closed quantum systems, symmetry-breaking transitions can be dual to topological transitions. Various aspects of topological matter have been generalized to open systems [85–90], e.g., zero-frequency edge modes with a finite lifetime can be protected via a *frequency gap* [91]. An open question remains whether edge modes with zero decay rate can be protected by a *dissipative gap*, resulting in a qubit steady state robust against local errors.

S.L. was supported by the NIST NRC Research Postdoctoral Associateship Award. R. B., J. T. Y., R. L., and A. V. G. acknowledge funding by the DOE ASCR Accelerated Research in Quantum Computing program (Award No. DE-SC0020312), NSF PFCQC program, DOE BES Materials and Chemical Sciences Research for Quantum Information Science program (Award No. DE-SC0019449), DOE ASCR Quantum Testbed Pathfinder program (Award No. DE-SC0019040), AFOSR, AFOSR MURI, ARO MURI, ARL CDQI, and NSF PFC at JQI. R. B. acknowledges support of NSERC and FRQNT of Canada.

- [1] H. Breuer and F. Petruccione, *The Theory of Open Quantum Systems* (Oxford University Press, New York, 2002).
- [2] C. Noh and D. G. Angelakis, *Rep. Prog. Phys.* **80**, 016401 (2016).
- [3] S. Diehl, A. Micheli, A. Kantian, B. Kraus, H. P. Büchler, and P. Zoller, *Nat. Phys.* **4**, 878 (2008).
- [4] J. F. Poyatos, J. I. Cirac, and P. Zoller, *Phys. Rev. Lett.* **77**, 4728 (1996).
- [5] M. B. Plenio and S. F. Huelga, *Phys. Rev. Lett.* **88**, 197901 (2002).
- [6] B. Buča and T. Prosen, *New J. Phys.* **14**, 073007 (2012).
- [7] V. V. Albert and L. Jiang, *Phys. Rev. A* **89**, 022118 (2014).
- [8] V. V. Albert, B. Bradlyn, M. Fraas, and L. Jiang, *Phys. Rev. X* **6**, 041031 (2016).
- [9] B. Buča, J. Tindall, and D. Jaksch, *Nat. Commun.* **10**, 1730 (2019).
- [10] D. Roberts and A. A. Clerk, *Phys. Rev. X* **10**, 021022 (2020).
- [11] K. Macieszczak, M. Guta, I. Lesanovsky, and J. P. Garrahan, *Phys. Rev. Lett.* **116**, 240404 (2016).
- [12] E. I. R. Chiacchio and A. Nunnenkamp, *Phys. Rev. Lett.* **122**, 193605 (2019).
- [13] S. Dutta and N. R. Cooper, arXiv:2004.07981.
- [14] Z.-P. Cian, G. Zhu, S.-K. Chu, A. Seif, W. DeGottardi, L. Jiang, and M. Hafezi, *Phys. Rev. Lett.* **123**, 063602 (2019).
- [15] M. van Caspel and V. Gritsev, *Phys. Rev. A* **97**, 052106 (2018).
- [16] M. Gau, R. Egger, A. Zazunov, and Y. Gefen, *Phys. Rev. B* **102**, 134501 (2020).
- [17] Z. Zhang, J. Tindall, J. Mur-Petit, D. Jaksch, and B. Buča, *J. Phys. A* **53**, 215304 (2020).
- [18] R. A. Santos, F. Iemini, A. Kamenev, and Y. Gefen, arXiv:2002.00237.
- [19] G. Lindblad, *Commun. Math. Phys.* **48**, 119 (1976).
- [20] V. Gorini, A. Kossakowski, and E. C. G. Sudarshan, *J. Math. Phys. (N.Y.)* **17**, 821 (1976).
- [21] A. Belavkin, B. Y. Zeldovich, A. Perelomov, and V. Popov, *Sov. Phys. JETP* **56**, 264 (1969).
- [22] V. V. Albert, Lindbladians with multiple steady states: Theory and applications, Ph.D. Thesis, Yale University, 2017.
- [23] D. A. Lidar, I. L. Chuang, and K. B. Whaley, *Phys. Rev. Lett.* **81**, 2594 (1998).
- [24] B. M. Terhal, *Rev. Mod. Phys.* **87**, 307 (2015).
- [25] M. Mirrahimi, Z. Leghtas, V. V. Albert, S. Touzard, R. J. Schoelkopf, L. Jiang, and M. H. Devoret, *New J. Phys.* **16**, 045014 (2014).
- [26] S. Puri, S. Boutin, and A. Blais, *npj Quantum Inf.* **3**, 18 (2017).
- [27] E. Kapit, *Phys. Rev. Lett.* **116**, 150501 (2016).
- [28] J. P. Paz and W. H. Zurek, *Proc. R. Soc. Ser. A* **454**, 355 (1998).
- [29] J. P. Barnes and W. S. Warren, *Phys. Rev. Lett.* **85**, 856 (2000).
- [30] C. Ahn, A. C. Doherty, and A. J. Landahl, *Phys. Rev. A* **65**, 042301 (2002).
- [31] M. Sarovar and G. J. Milburn, *Phys. Rev. A* **72**, 012306 (2005).

- [32] O. Oreshkov and T. A. Brun, *Phys. Rev. A* **76**, 022318 (2007).
- [33] J. Kerckhoff, H. I. Nurdin, D. S. Pavlichin, and H. Mabuchi, *Phys. Rev. Lett.* **105**, 040502 (2010).
- [34] J.-M. Lihm, K. Noh, and U. R. Fischer, *Phys. Rev. A* **98**, 012317 (2018).
- [35] S. Sachdev, *Quantum Phase Transitions*, 2nd ed. (Cambridge University Press, Cambridge, England, 2011).
- [36] P. Kirton, M. M. Roses, J. Keeling, and E. G. Dalla Torre, *Adv. Quantum Technol.* **2**, 1800043 (2019).
- [37] A. Mitra, S. Takei, Y. B. Kim, and A. J. Millis, *Phys. Rev. Lett.* **97**, 236808 (2006).
- [38] D. Nagy, G. Szirmai, and P. Domokos, *Phys. Rev. A* **84**, 043637 (2011).
- [39] J. Marino and S. Diehl, *Phys. Rev. Lett.* **116**, 070407 (2016).
- [40] E. G. Dalla Torre, E. Demler, T. Giamarchi, and E. Altman, *Phys. Rev. B* **85**, 184302 (2012).
- [41] E. G. Dalla Torre, S. Diehl, M. D. Lukin, S. Sachdev, and P. Strack, *Phys. Rev. A* **87**, 023831 (2013).
- [42] M. F. Maghrebi and A. V. Gorshkov, *Phys. Rev. B* **93**, 014307 (2016).
- [43] J. T. Young, A. V. Gorshkov, M. Foss-Feig, and M. F. Maghrebi, *Phys. Rev. X* **10**, 011039 (2020).
- [44] R. Lundgren, A. V. Gorshkov, and M. F. Maghrebi, *Phys. Rev. A* **102**, 032218 (2020).
- [45] C. Joshi, F. Nissen, and J. Keeling, *Phys. Rev. A* **88**, 063835 (2013).
- [46] J. Jin, A. Biella, O. Viyuela, C. Ciuti, R. Fazio, and D. Rossini, *Phys. Rev. B* **98**, 241108(R) (2018).
- [47] M. H. Szymanska, J. Keeling, and P. B. Littlewood, *Phys. Rev. Lett.* **96**, 230602 (2006).
- [48] R. Rota, F. Minganti, C. Ciuti, and V. Savona, *Phys. Rev. Lett.* **122**, 110405 (2019).
- [49] W. Verstraelen, R. Rota, V. Savona, and M. Wouters, *Phys. Rev. Research* **2**, 022037 (2020).
- [50] S. R. K. Rodriguez, W. Casteels, F. Storme, N. Carlon Zambon, I. Sagnes, L. Le Gratiet, E. Galopin, A. Lemaître, A. Amo, C. Ciuti, and J. Bloch, *Phys. Rev. Lett.* **118**, 247402 (2017).
- [51] C. Carr, R. Ritter, C. G. Wade, C. S. Adams, and K. J. Weatherill, *Phys. Rev. Lett.* **111**, 113901 (2013).
- [52] M. Fitzpatrick, N. M. Sundaresan, A. C. Y. Li, J. Koch, and A. A. Houck, *Phys. Rev. X* **7**, 011016 (2017).
- [53] J. Klinder, H. Keßler, M. Wolke, L. Mathey, and A. Hemmerich, *Proc. Natl. Acad. Sci. U.S.A.* **112**, 3290 (2015).
- [54] F. Brennecke, R. Mottl, K. Baumann, R. Landig, T. Donner, and T. Esslinger, *Proc. Natl. Acad. Sci. U.S.A.* **110**, 11763 (2013).
- [55] F. Minganti, A. Biella, N. Bartolo, and C. Ciuti, *Phys. Rev. A* **98**, 042118 (2018).
- [56] H. Wilming, M. J. Kastoryano, A. H. Werner, and J. Eisert, *J. Math. Phys.* (N.Y.) **58**, 033302 (2017).
- [57] E. M. Kessler, G. Giedke, A. Imamoglu, S. F. Yelin, M. D. Lukin, and J. I. Cirac, *Phys. Rev. A* **86**, 012116 (2012).
- [58] Z. Leghtas, S. Touzard, I. M. Pop, A. Kou, B. Vlastakis, A. Petrenko, K. M. Sliwa, A. Narla, S. Shankar, M. J. Hatridge *et al.*, *Science* **347**, 853 (2015).
- [59] N. Bartolo, F. Minganti, W. Casteels, and C. Ciuti, *Phys. Rev. A* **94**, 033841 (2016).
- [60] F. Minganti, N. Bartolo, J. Lolli, W. Casteels, and C. Ciuti, *Sci. Rep.* **6**, 26987 (2016).
- [61] H. J. Carmichael, *Phys. Rev. X* **5**, 031028 (2015).
- [62] J. B. Curtis, I. Boettcher, J. T. Young, M. F. Maghrebi, H. Carmichael, A. V. Gorshkov, and M. Foss-Feig, [arXiv:2006.05593](https://arxiv.org/abs/2006.05593).
- [63] See Supplemental Material at <http://link.aps.org/supplemental/10.1103/PhysRevLett.125.240405> for calculations supporting dissipative-gap closure at the phase boundary, numerical evidence for a noiseless subsystem in the strong-broken phase, and a discussion on passive protection of a classical bit in the weak-broken phase, which includes Refs. [64–66].
- [64] T. Prosen, *New J. Phys.* **10**, 043026 (2008).
- [65] T. Prosen and T. H. Seligman, *J. Phys. A* **43**, 392004 (2010).
- [66] R. Blume-Kohout, H. K. Ng, D. Poulin, and L. Viola, *Phys. Rev. A* **82**, 062306 (2010).
- [67] X. H. Zhang and H. U. Baranger, [arXiv:2007.01422](https://arxiv.org/abs/2007.01422).
- [68] L. Gilles, B. M. Garraway, and P. L. Knight, *Phys. Rev. A* **49**, 2785 (1994).
- [69] J. Cohen, Autonomous quantum error correction with superconducting qubits, Ph.D. Thesis, Ecole Normale Supérieure, 2017.
- [70] E. Knill, R. Laflamme, and L. Viola, *Phys. Rev. Lett.* **84**, 2525 (2000).
- [71] Y. Wang, M. Um, J. Zhang, S. An, M. Lyu, J.-N. Zhang, L. M. Duan, D. Yum, and K. Kim, *Nat. Photonics* **11**, 646 (2017).
- [72] R. Belyansky, J. T. Young, P. Bienias, Z. Eldredge, A. M. Kaufman, P. Zoller, and A. V. Gorshkov, *Phys. Rev. Lett.* **123**, 213603 (2019).
- [73] I. Reichenbach and I. H. Deutsch, *Phys. Rev. Lett.* **99**, 123001 (2007).
- [74] A. V. Gorshkov, A. M. Rey, A. J. Daley, M. M. Boyd, J. Ye, P. Zoller, and M. D. Lukin, *Phys. Rev. Lett.* **102**, 110503 (2009).
- [75] R. W. Heeres, P. Reinhold, N. Ofek, L. Frunzio, L. Jiang, M. H. Devoret, and R. J. Schoelkopf, *Nat. Commun.* **8**, 94 (2017).
- [76] N. Ofek, A. Petrenko, R. Heeres, P. Reinhold, Z. Leghtas, B. Vlastakis, Y. Liu, L. Frunzio, S. M. Girvin, L. Jiang, M. Mirrahimi, M. H. Devoret, and R. J. Schoelkopf, *Nature (London)* **536**, 441 (2016).
- [77] R. Lescanne, M. Villiers, T. Peronnin, A. Sarlette, M. Delbecq, B. Huard, T. Kontos, M. Mirrahimi, and Z. Leghtas, *Nat. Phys.* **16**, 509 (2020).
- [78] S. Touzard, A. Grimm, Z. Leghtas, S. O. Mundhada, P. Reinhold, C. Axline, M. Reagor, K. Chou, J. Blumoff, K. M. Sliwa, S. Shankar, L. Frunzio, R. J. Schoelkopf, M. Mirrahimi, and M. H. Devoret, *Phys. Rev. X* **8**, 021005 (2018).
- [79] A. Grimm, N. E. Frattini, S. Puri, S. O. Mundhada, S. Touzard, M. Mirrahimi, S. M. Girvin, S. Shankar, and M. H. Devoret, *Nature (London)* **584**, 205 (2020).
- [80] J. M. Gertler, B. Baker, J. Li, S. Shirol, J. Koch, and C. Wang, [arXiv:2004.09322](https://arxiv.org/abs/2004.09322).
- [81] J. Guillaud and M. Mirrahimi, *Phys. Rev. X* **9**, 041053 (2019).
- [82] V. V. Albert, S. O. Mundhada, A. Grimm, S. Touzard, M. H. Devoret, and L. Jiang, *Quantum Sci. Technol.* **4**, 035007 (2019).
- [83] V. V. Albert, J. P. Covey, and J. Preskill, *Phys. Rev. X* **10**, 031050 (2020).

- [84] S. C. Burd, R. Srinivas, J. J. Bollinger, A. C. Wilson, D. J. Wineland, D. Leibfried, D. H. Slichter, and D. T. C. Allcock, *Science* **364**, 1163 (2019).
- [85] E. J. Bergholtz, J. C. Budich, and F. K. Kunst, [arXiv:1912.10048](#).
- [86] A. Altland, M. Fleischhauer, and S. Diehl, [arXiv:2007.10448](#).
- [87] F. Song, S. Yao, and Z. Wang, *Phys. Rev. Lett.* **123**, 170401 (2019).
- [88] C.-H. Liu, K. Zhang, Z. Yang, and S. Chen, *Phys. Rev. Research* **2**, 043167 (2020).
- [89] T. Yoshida, K. Kudo, H. Katsura, and Y. Hatsugai, *Phys. Rev. Research* **2**, 033428 (2020).
- [90] C. Gneiting, A. Koottandavida, A. V. Rozhkov, and F. Nori, [arXiv:2007.05960](#).
- [91] S. Lieu, M. McGinley, and N. R. Cooper, *Phys. Rev. Lett.* **124**, 040401 (2020).

Supplemental Material for “Symmetry breaking and error correction in open quantum systems”

Simon Lieu,^{1,2} Ron Belyansky,^{1,2} Jeremy T. Young,¹ Rex Lundgren,^{1,2} Victor V. Albert,^{3,4} Alexey V. Gorshkov^{1,2}

¹*Joint Quantum Institute, NIST/University of Maryland, College Park, MD 20742, USA*

²*Joint Center for Quantum Information and Computer Science,
NIST/University of Maryland, College Park, Maryland 20742 USA*

³*Institute for Quantum Information and Matter and Walter Burke Institute for
Theoretical Physics, California Institute of Technology, Pasadena, CA 91125, USA*

⁴*National Institute of Standards and Technology, Gaithersburg, MD 20899, USA*

In Sec. 1, we analytically show that the dissipative gap closes at the critical point by utilizing an exact solution for the Lindblad spectrum [Fig. 1(b) in the main text]. Sec. 2 exhibits numerical evidence for a noiseless subsystem steady state in the strong-broken phase (away from \mathcal{L}_0). Sec. 3 tracks the evolution of the state throughout the error protocol in the main text. We show numerical evidence for the state structure defined in Eq. (5) of the main text for errors which keep the model in the strong-broken phase. Sec. 4 uses the asymptotic projection method to confirm perfect fidelity recovery in the thermodynamic limit, in agreement with the direct numerical evolution discussed in the main text. In Sec. 5 we show that a *classical bit* encoded into the steady state is protected against perturbations which keep the Lindbladian in the *weak-broken* phase.

1. CLOSING OF THE DISSIPATIVE GAP AT THE CRITICAL POINT

We show that an extensive number of spectral eigenvalues touch zero at the critical boundary [Fig. 1(a) in the main text] when approaching from the unbroken phase in the thermodynamic limit. We utilize Prosen’s “third quantization” technique which allows us to fully diagonalize a quadratic Lindbladian [S1, S2]. For the Hamiltonian (3) in the presence of one-photon loss only (i.e. the weak transition), the Lindbladian can be expressed as $\mathcal{L} = \epsilon_+ \beta_+^\dagger \beta_+ + \epsilon_- \beta_-^\dagger \beta_-$, where β are bosonic superoperators satisfying generalized commutation relations $[\beta_i', \beta_j^\dagger] = \delta_{ij}$. These excite a quantum of “complex energy” $\epsilon_\pm = -\kappa_\pm \pm \sqrt{4\lambda^2 - \omega^2}$, where the (unique) steady state is annihilated by all quasiparticles $\beta_\pm' \rho_{ss} = 0$, and the many-body spectrum is built from these single-particle excitations $\mathcal{L}[(\beta_+^\dagger)^n (\beta_-^\dagger)^m \rho_{ss}] = (n\epsilon_+ + m\epsilon_-)[(\beta_+^\dagger)^n (\beta_-^\dagger)^m \rho_{ss}]$. The single-particle spectrum touches zero at $\kappa_1/\omega = \sqrt{4(\lambda/\omega)^2 - 1}$, which coincides with the emergence of a non-zero order parameter (see main text). This implies that an infinite number of eigenvalues of \mathcal{L} are zero at the critical point of the weak transition from 1 steady state to 2 steady states. We plot both the single-particle spectrum and match it with many-body numerics in Fig. S1. [Fig. S1(a) and Fig. 1(b) are equivalent; here we plot the real and imaginary parts side by side.] The numerical spectrum deviates from analytical predictions only near the critical boundary due to truncation of the Hilbert space dimension. Note that the analytical and numerical plots are only valid in the unbroken phase. The steady state has an infinite number of photons in the broken phase, hence any finite-size Hilbert space will not produce a converged spectrum. Finite-size scaling [Fig. 1(d)] suggests that two eigenvalues are exponentially close to zero in the weak-broken phase with a dissipative gap to the rest of the modes.

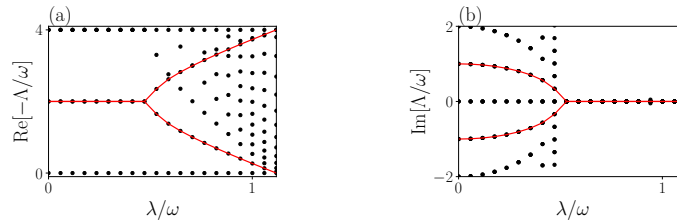


FIG. S1. Analytical single-particle spectrum (red lines) and numerical many-body spectrum (black dots) with $\kappa_1/\omega = 2$, $\kappa_2 = \kappa_d = 0$. The many-body spectrum comes in integer multiples of the single-particle excitations. As the system approaches the critical point from the unbroken phase, the single-particle spectrum touches zero at the phase boundary $\lambda/\omega \approx 1.1$. The numerical spectrum starts to deviate from the analytical predictions near the transition due to truncation of the Hilbert space dimension $d_{\text{Hilbert}} = 70$. We plot up to 25 eigenvalues closest to zero for clarity.

2. NOISELESS SUBSYSTEM IN THE STRONG-BROKEN PHASE

We demonstrate that the model described in the main text possesses a qubit steady-state structure in the thermodynamic limit of the strong-broken phase. In particular, we will show that the four right eigenoperators with zero eigenvalue can be written in the form $r_{\mu\nu} = |\mu\rangle\langle\nu| \otimes z$ with $(\mu, \nu) \in (+, -)$. This is called a noiseless subsystem (NS) if z is mixed, and a decoherence-free subspace (DFS) if z is pure [S3–S5].

The four steady-state right eigenoperators belonging to the different parity sectors are

$$r_{++}^F = \begin{pmatrix} s_{++} & 0 \\ 0 & 0 \end{pmatrix}, \quad r_{--}^F = \begin{pmatrix} 0 & 0 \\ 0 & s_{--} \end{pmatrix}, \quad r_{+-}^F = \begin{pmatrix} 0 & s_{+-} \\ 0 & 0 \end{pmatrix}, \quad r_{-+}^F = \begin{pmatrix} 0 & 0 \\ s_{-+} & 0 \end{pmatrix} \quad (\text{S1})$$

in the Fock basis $[|0\rangle, |2\rangle, |4\rangle, \dots, |1\rangle, |3\rangle, |5\rangle, \dots]^T$. They each satisfy $\mathcal{L}(r) = 0$ (in the thermodynamic limit). Since s_{++}, s_{--} are guaranteed to be Hermitian matrices, we can diagonalize them via a unitary transformation $U = \text{Diag}[U_+, U_-]$ which relates the Fock basis to the diagonal basis $r_i^d = U^\dagger r_i^F U$. In this new basis, the eigenoperators are

$$r_{++}^d = \begin{pmatrix} z_{++} & 0 \\ 0 & 0 \end{pmatrix}, \quad r_{--}^d = \begin{pmatrix} 0 & 0 \\ 0 & z_{--} \end{pmatrix}, \quad r_{+-}^d = \begin{pmatrix} 0 & z_{+-} \\ 0 & 0 \end{pmatrix}, \quad r_{-+}^d = \begin{pmatrix} 0 & 0 \\ z_{-+} & 0 \end{pmatrix}, \quad (\text{S2})$$

where z_{++}, z_{--} are diagonal by construction, and z_{+-}, z_{-+} are diagonal in the thermodynamic limit. We will show that $z_{++} = z_{--} = z_{+-} = z_{-+}$ in this limit, which implies that the system hosts a NS or a DFS.

In the special limit $\omega = \kappa_d = \kappa_1 = 0, \lambda \neq 0, \kappa_2 \neq 0$, any pure superposition of even and odd cat states remains steady, as discussed in the main text. Thus $z_{++} = z_{--} = z_{+-} = z_{-+} = \text{Diag}[1, 0, 0, 0, \dots]$, which implies a DFS.

We now consider a parameter regime away from this limit but within the strong-broken phase. We start by adding dephasing: $\omega = \kappa_1 = 0, \kappa_d \neq 0, \lambda \neq 0, \kappa_2 \neq 0$. We will numerically show that the z matrices are equal and not pure. For the matrix distance, we choose the trace distance $D_t(A, B) = \text{Tr}[\sqrt{(A - B)^2}]/2$. In Fig. S2(a,b), we plot $D_t(z_{++}, z_{--})$ and $D_t(z_{++}, z_{+-})$ as the system approaches the thermodynamic limit $\lambda/\kappa_2 = N \rightarrow \infty$. Indeed, we find that the matrices z_{++}, z_{--}, z_{+-} all converge to a single matrix as N is increased. (z_{+-} and z_{-+} are related by Hermiticity.) Additionally, in Fig. S2(c), we show that z_{++} is a non-pure matrix with elements that fall off as $(z_{++})_{ii} \sim \exp[-i]$. The purity of z_{++} *degrades* with N (not shown). We conclude that the system tends to a noiseless subsystem in the thermodynamic limit, since the $z_{\pm\pm}$ all converge to a single non-pure matrix. [For completeness, in Fig. S2(d), we show that the smallest eigenvalue in the off-diagonal sector indeed tends to zero exponentially quickly with N . The steady-state degeneracy is split by an exponentially small factor, characteristic of symmetry-breaking transitions.]

We repeat this analysis in the limit of no dephasing but non-zero ω : $\kappa_d = \kappa_1 = 0, \omega \neq 0, \lambda \neq 0, \kappa_2 \neq 0$. Fig. S3 shows that the $z_{\pm\pm}$ converge to a single non-pure matrix in the thermodynamic limit, similar to the case of dephasing. We therefore conclude that a generic model in the strong-broken phase possesses a noiseless subsystem, whilst a decoherence-free subspace exists at a special point \mathcal{L}_0 in the phase diagram.

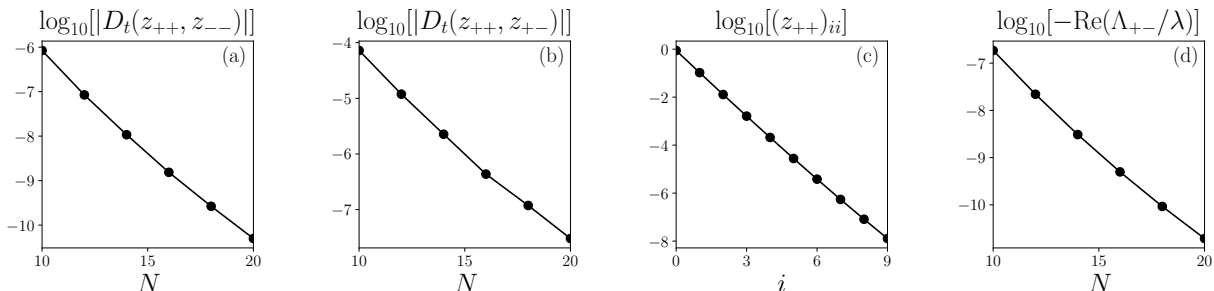


FIG. S2. Parameters: $\lambda/\kappa_2 = N, \kappa_d/\lambda = 0.03, \omega = \kappa_1 = 0$, i.e. non-zero dephasing. (a,b) The trace norm $D_t(A, B) = \text{Tr}[\sqrt{(A - B)^2}]/2$ between the different right eigenoperators with zero eigenvalue goes to zero in the thermodynamic limit $N \rightarrow \infty$. (c) Diagonal matrix elements of z_{++} for $N = 20$. The matrix is not pure, with elements scaling as $(z_{++})_{ii} \sim \exp[-ci]$ for some $c > 0$. (d) The off-diagonal symmetry sector of the Lindbladian acquires an eigenvalue of zero as $N \rightarrow \infty$. Here Λ_{+-} is the smallest eigenvalue in the off-diagonal sector.

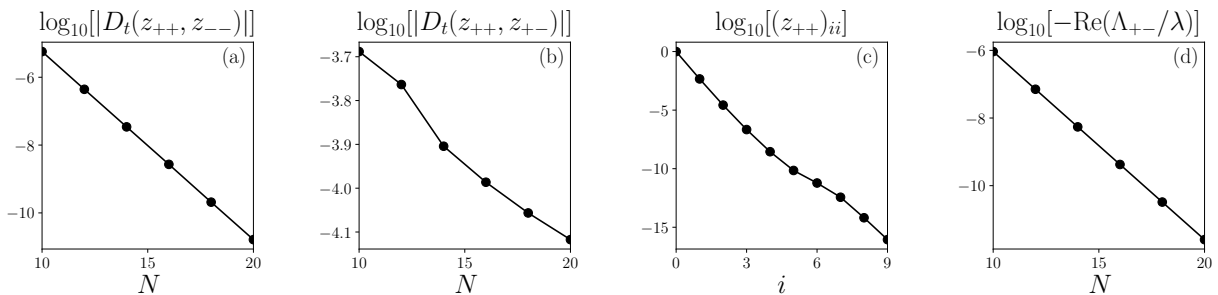


FIG. S3. Parameters: $\lambda/\kappa_2 = N, \omega/\lambda = 0.5, \kappa_d = \kappa_1 = 0$. (a,b) The trace norm between the different right eigenoperators with zero eigenvalue goes to zero in the thermodynamic limit $N \rightarrow \infty$. (c) Diagonal matrix elements of z_{++} for $N = 20$. The matrix is not pure, with elements scaling as $(z_{++})_{ii} \sim \exp[-ci]$ for some $c > 0$. (d) The off-diagonal symmetry sector of the Lindbladian acquires an eigenvalue of zero as $N \rightarrow \infty$. Here Λ_{+-} is the smallest eigenvalue in the off-diagonal sector.

3. EVOLUTION FROM DECOHERENCE-FREE SUBSPACE TO NOISELESS SUBSYSTEM

We now track the state throughout the error protocol described in the main text for both dephasing errors and Hamiltonian-frequency errors. Our analysis will confirm that the state can be written as a qubit tensored with a mixed state throughout the entire quench protocol, i.e. the structure described in Eq. (5) in the main text. An analytical understanding of this mechanism requires an exact solution for the steady states in the entire strong-broken phase—an important direction for future work.

We prepare the system in a pure steady state of \mathcal{L}_0 :

$$\rho_i = \begin{pmatrix} |c_e|^2 & c_e c_o^* \\ c_e^* c_o & |c_o|^2 \end{pmatrix} \quad (\text{S3})$$

in the basis of even and odd cat states $|\alpha\rangle_e, |\alpha\rangle_o$, where $|c_e|^2 + |c_o|^2 = 1$ and $\mathcal{L}_0(\rho_i) = 0$. We evolve this initial state with an error to a “middle” state

$$\rho_m(\tau_q) = e^{(\mathcal{L}_0 + \mathcal{L}')\tau_q} \rho_i. \quad (\text{S4})$$

We wish to show that this middle state can be written in the form

$$\rho_m(\tau_q) = \begin{pmatrix} |c_e|^2 & c_e c_o^* \\ c_e^* c_o & |c_o|^2 \end{pmatrix} \otimes M \quad (\text{S5})$$

for some M which is not necessarily pure.

We numerically solve for $\rho_m(\tau_q)$ via Eq. (S4) for arbitrary quench times and $\mathcal{L}_0 + \mathcal{L}'$ in the strong-broken phase. We then split the matrix up into symmetry sectors in the Fock basis $\rho_m = |c_e|^2 \rho_{++}^F + |c_o|^2 \rho_{--}^F + (c_e c_o^* \rho_{+-}^F + h.c.)$. The four operators belonging to the different parity sectors are

$$\rho_{++}^F = \begin{pmatrix} x_{++} & 0 \\ 0 & 0 \end{pmatrix}, \quad \rho_{--}^F = \begin{pmatrix} 0 & 0 \\ 0 & x_{--} \end{pmatrix}, \quad \rho_{+-}^F = \begin{pmatrix} 0 & x_{+-} \\ 0 & 0 \end{pmatrix}, \quad \rho_{-+}^F = \begin{pmatrix} 0 & 0 \\ x_{-+} & 0 \end{pmatrix} \quad (\text{S6})$$

in the Fock basis $[|0\rangle, |2\rangle, |4\rangle, \dots, |1\rangle, |3\rangle, |5\rangle, \dots]^T$. Since x_{++}, x_{--} are guaranteed to be Hermitian matrices, we can diagonalize them via a unitary transformation $V = \text{Diag}[V_+, V_-]$ which relates the Fock basis to the diagonal basis $\rho_i^d = V^\dagger \rho_i^F V$. In this new basis, the eigenoperators are

$$\rho_{++}^d = \begin{pmatrix} M_{++} & 0 \\ 0 & 0 \end{pmatrix}, \quad \rho_{--}^d = \begin{pmatrix} 0 & 0 \\ 0 & M_{--} \end{pmatrix}, \quad \rho_{+-}^d = \begin{pmatrix} 0 & M_{+-} \\ 0 & 0 \end{pmatrix}, \quad \rho_{-+}^d = \begin{pmatrix} 0 & 0 \\ M_{-+} & 0 \end{pmatrix}, \quad (\text{S7})$$

where all the M s are diagonal by construction. We now show that all M s converge to a single matrix in the thermodynamic limit, confirming the form of Eq. (S5).

We plot the trace distance between the different M s for both short and long quench times $\tau_q \lambda \in [10^{-2}, 10^2]$. In Fig. S4, we consider a quench in the dephasing strength. Indeed, the trace distance between the different M s goes to zero exponentially fast as a function of N , which suggests that the ansatz in Eq. (S5) is correct in the limit $N \rightarrow \infty$.

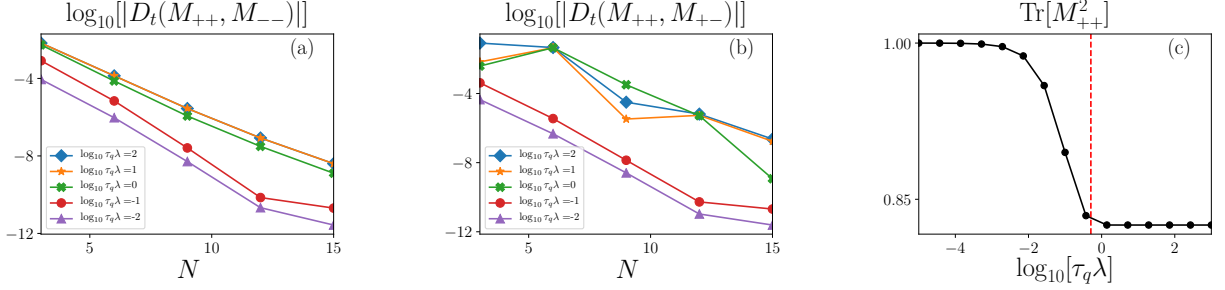


FIG. S4. Parameters: $\lambda/\kappa_2 = N, \kappa_d/\lambda = 0.03, \omega = \kappa_1 = 0, c_e = 1/\sqrt{2}, c_o = i/\sqrt{2}$. (a) The trace distance between M_{++} and M_{--} goes to zero exponentially fast in N . (b) Analogous behavior is observed for M_{++} and M_{+-} . (c) $N = 15$, the red line is the time scale set by the inverse dissipative gap $\tau_g = \Delta_g^{-1}$ of $\mathcal{L}_0 + \mathcal{L}'$. The state is approximately pure for short quenches compared to this time scale, while it settles to its (mixed) steady-state value for quenches longer than this timescale.

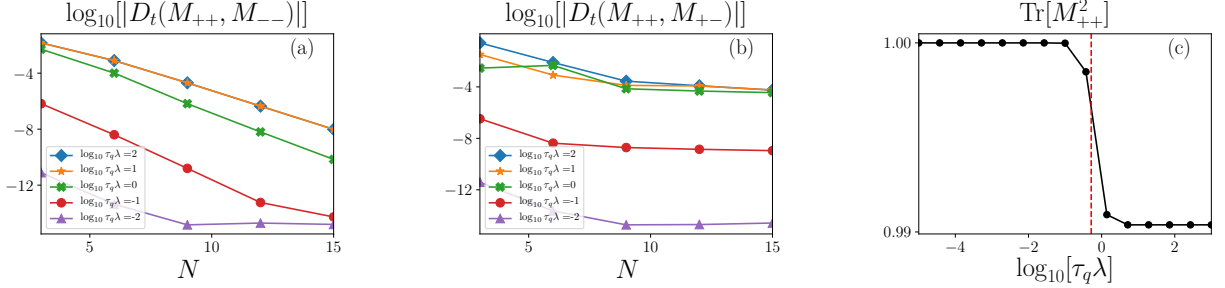


FIG. S5. Parameters: $\lambda/\kappa_2 = N, \omega/\lambda = 0.5, \kappa_d = \kappa_1 = 0, c_e = 1/\sqrt{2}, c_o = i/\sqrt{2}$. (a) The trace distance between M_{++} and M_{--} goes to zero exponentially fast in N . (b) Analogous behavior is observed for M_{++} and M_{+-} . (c) $N = 15$, the red line is the time scale set by the inverse dissipative gap $\tau_g = \Delta_g^{-1}$ of $\mathcal{L}_0 + \mathcal{L}'$. The state is approximately pure for short quenches compared to this time scale, while it settles to its (mixed) steady-state value for quenches longer than this timescale.

We also track the purity of this matrix: At quench times that are short compared to the timescale set by the dissipative gap (red line), the middle state remains approximately pure, whilst longer quenches imply that the system settles into its new steady state, which is mixed (see previous section). Analogous behavior is observed for a quench in frequency (Fig. S5).

4. ASYMPTOTIC PROJECTION

We verify the perfect recovery of the fidelity observed in Fig. 2 of the main text via the asymptotic projection method [S6]. Fig. 2 shows that qubit cat states will self correct via the environment if $\mathcal{L}_0 + \mathcal{L}'$ remains in the strong symmetry-broken phase. This behavior can be understood via perturbation theory for short quenches (compared to the time scale set by the dissipative gap) [S7]. Here, we consider long quench times where the system evolves into the steady state of $\mathcal{L}_0 + \mathcal{L}'$. Remarkably, such a drastic error can still be passively corrected via the environment \mathcal{L}_0 . We provide simple expressions relating the initial, intermediate, and final states by projecting onto the corresponding steady state manifolds.

Defining our initial state as ρ_i , we evolve it with an error ($\mathcal{L}_0 + \mathcal{L}'$) to a “middle” state $\rho_m(\tau_q) = e^{(\mathcal{L}_0 + \mathcal{L}')\tau_q} \rho_i$. We then evolve the state with \mathcal{L}_0 for an infinite time to reach the final state $\rho_f(\tau_q) = \lim_{\tau \rightarrow \infty} e^{\mathcal{L}_0 \tau} \rho_m(\tau_q)$. We will discuss how $\rho_{i,m,f}$ relate to one another in this protocol when τ_q is much longer than the inverse dissipative gap of $\mathcal{L}_0 + \mathcal{L}'$.

We first prepare the system in a pure steady state of \mathcal{L}_0 ,

$$\rho_i = |a|^2 r_{++}^0 + |b|^2 r_{--}^0 + a^* b r_{+-}^0 + a b^* r_{-+}^0, \quad (\text{S8})$$

where $r_{++}^0 = |\alpha\rangle_e \langle \alpha|_e$, $r_{--}^0 = |\alpha\rangle_o \langle \alpha|_o$, $r_{+-}^0 = |\alpha\rangle_e \langle \alpha|_o$, $r_{-+}^0 = |\alpha\rangle_o \langle \alpha|_e$; $|\alpha\rangle_{e/o}$ is the even/odd cat state, and $\mathcal{L}_0(r_{\pm\pm}^0) = 0$. To find ρ_m , it is useful to define the right and left eigenoperators of the error:

$$(\mathcal{L}_0 + \mathcal{L}')(\tilde{r}_j) = \tilde{\Lambda}_j(\tilde{r}_j), \quad (\mathcal{L}_0^\dagger + \mathcal{L}'^\dagger)(\tilde{l}_j) = \tilde{\Lambda}_j^*(\tilde{l}_j), \quad (\text{S9})$$

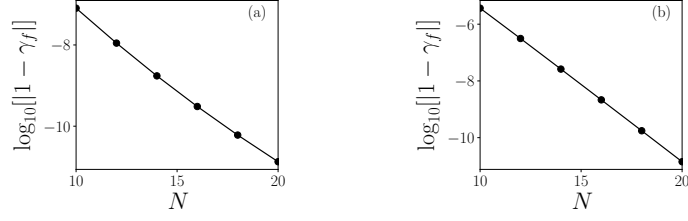


FIG. S6. Scaling of $|1 - \gamma_f|$ as a function of N for (a) a dephasing error $\lambda/\kappa_2 = N, \kappa_d/\lambda = 0.03$ and (b) a frequency error $\lambda/\kappa_2 = N, \omega/\lambda = 0.03$. γ_f approaches one exponentially fast in N for both cases.

where the spectrum $\{\tilde{\Lambda}\}$ and eigenoperators determine the dynamics under $\mathcal{L}_0 + \mathcal{L}'$. Assuming that the error keeps the system in the strong-broken phase, we know that two eigenvalues will be exactly zero $\tilde{\Lambda}_{++}^0 = \tilde{\Lambda}_{--}^0 = 0$ and two eigenvalues will be exponentially close to zero $\tilde{\Lambda}_{+-}^0 = (\tilde{\Lambda}_{-+}^0)^* \sim e^{-N}$. We label the eigenvalue of the first “excited” state (above these four) as $\tilde{\Lambda}_g$, which sets the dissipative gap in the thermodynamic limit. The exact expression for $\rho_m(\tau_q)$ reads

$$\rho_m(\tau_q) = \sum_j \exp[\tilde{\Lambda}_j \tau_q] \text{Tr}[\tilde{l}_j^\dagger \rho_i] \tilde{r}_j, \quad (\text{S10})$$

where we have used the orthogonality relation $\text{Tr}[\tilde{l}_j^\dagger \tilde{r}_k] = \delta_{jk}$. $-\text{Re}[\tilde{\Lambda}_g^{-1}]$ sets the lifetime of each eigenoperator. Consider a quench time that obeys $-\text{Re}[\tilde{\Lambda}_g^{-1}] \ll \tau_q \ll -\text{Re}[(\tilde{\Lambda}_{+-}^0)^{-1}] \sim e^N$. This quench is long enough for the system to relax into the new steady state but not so long that coherences are lost. In this regime, ρ_m will tend to the following matrix t_m

$$\lim_{N \rightarrow \infty} \rho_m(\tau_q) = t_m, \quad t_m = |a|^2 \tilde{r}_{++}^0 + |b|^2 \tilde{r}_{--}^0 + [a^* b \gamma_m \tilde{r}_{+-}^0 + h.c.], \quad \gamma_m = \text{Tr}[(\tilde{l}_{+-}^0)^\dagger r_{+-}^0]. \quad (\text{S11})$$

If τ_q is longer than $-\text{Re}[\tilde{\Lambda}_g^{-1}]$, then all excitations will vanish and we will be left with the projection onto the steady-state manifold of the error. We have confirmed this numerically by doing the full time evolution $\rho_m = \exp[(\mathcal{L} + \mathcal{L}')\tau_q] \rho_i$ and comparing the resulting matrix with t_m . Indeed, the trace distance $D_t(\rho_m, t_m) = \text{Tr}[\sqrt{(\rho_m - t_m)^2}/2]$ goes to zero exponentially quickly in N . We have thus found a simple expression for $\rho_m(\tau_q)$ for this range of τ_q .

Having understood the structure of this intermediate state, $\rho_m \approx t_m$, we now project this state back onto the steady-state manifold of \mathcal{L}_0 . Without any additional approximations, the resulting state is

$$\lim_{N \rightarrow \infty} \rho_f = |a|^2 r_{++}^0 + |b|^2 r_{--}^0 + \gamma_f a^* b r_{+-}^0 + \gamma_f^* a b^* r_{-+}^0, \quad \gamma_f = \text{Tr}[(\tilde{l}_{+-}^0)^\dagger r_{+-}^0] \text{Tr}[(l_{+-}^0)^\dagger \tilde{r}_{+-}^0]. \quad (\text{S12})$$

We see that the final state is very simply related to the initial state via the γ_f parameter in Eq. (S12). Moreover, numerically we observe that γ_f approaches 1 exponentially fast in the thermodynamic limit, depicted in Fig. S6 for both the case of (a) $\kappa_d \neq 0$ and (b) $\omega \neq 0$. (We have also checked that γ_m approaches 1 in the same limit.) This implies that the final state ρ_f is indeed expected to return to its initial (pure) state ρ_i in the thermodynamic limit.

Structure of the left eigenoperators \tilde{l}

In Sec. 3 and earlier in this Section, we saw that the initial state settles into the noiseless subsystem of the intermediate Lindbladian $\mathcal{L}_0 + \mathcal{L}'$ without losing any coherences as $N \rightarrow \infty$. We would like to find a simple explanation for this behavior. This evolution would be accounted for (in the limit $N \rightarrow \infty$) if the left eigenoperators of $\mathcal{L}_0 + \mathcal{L}'$ with zero eigenvalue are equal to the identity in each symmetry sector, since, in this case, $\gamma_m = \text{Tr}[(l_{+-}^0)^\dagger \tilde{r}_{+-}^0] = \text{Tr}[\tilde{s}_{+-}^0] = \text{Tr}[\tilde{z}_{+-}^0] = 1$ where in the last step we have used $\text{Tr}[\tilde{z}_{+-}^0] = \text{Tr}[\tilde{z}_{++}^0] = 1$. (See Sec. 2 for definitions of r, s, z .) We will show that this is indeed true. Splitting up the left eigenoperators into symmetry sectors, we have

$$\tilde{l}_{++}^F = \begin{pmatrix} y_{++} & 0 \\ 0 & 0 \end{pmatrix}, \quad \tilde{l}_{--}^F = \begin{pmatrix} 0 & 0 \\ 0 & y_{--} \end{pmatrix}, \quad \tilde{l}_{+-}^F = \begin{pmatrix} 0 & y_{+-} \\ 0 & 0 \end{pmatrix}, \quad \tilde{l}_{-+}^F = \begin{pmatrix} 0 & 0 \\ y_{-+} & 0 \end{pmatrix}. \quad (\text{S13})$$

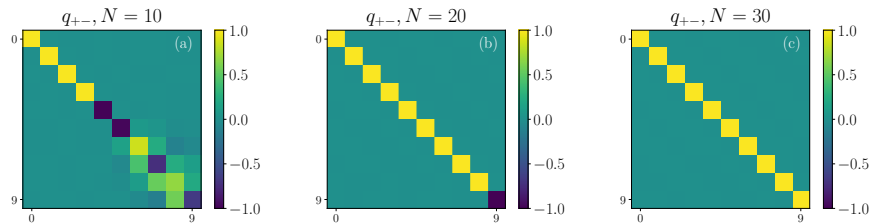


FIG. S7. Plot of a 10×10 block of q_{+-} ; all elements are real. Parameters: $\kappa_2/\lambda = 1/N$, $\kappa_d/\lambda = 0.03$, $\omega = \kappa_1 = 0$. As the system approaches the thermodynamic limit, the matrix tends to the identity.

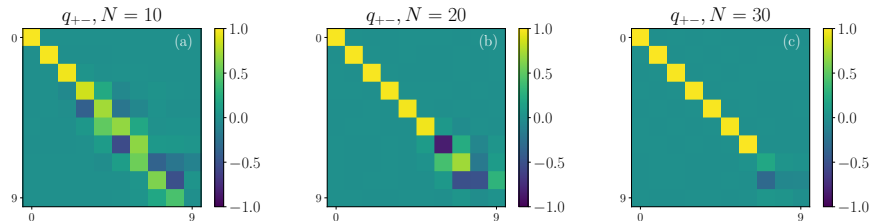


FIG. S8. Plot of a 10×10 block of q_{+-} ; all elements are real. Parameters: $\kappa_2/\lambda = 1/N$, $\omega/\lambda = 0.5$, $\kappa_d = \kappa_1 = 0$. As the system approaches the thermodynamic limit, the matrix tends to the identity.

As before, we are in the Fock basis $[|0\rangle, |2\rangle, |4\rangle, \dots, |1\rangle, |3\rangle, |5\rangle, \dots]^T$. Then $y_{++} = y_{--} = \mathbb{I}$ since any arbitrary initial state must have unit overlap with the steady-state solutions with non-zero trace. Now we switch from the Fock basis to the diagonal basis of r , $r_i^d = U^\dagger r_i^F U$, $\tilde{l}_i^d = U^\dagger \tilde{l}_i^F U$, and obtain

$$\tilde{l}_{++}^d = \begin{pmatrix} q_{++} & 0 \\ 0 & 0 \end{pmatrix}, \quad \tilde{l}_{--}^d = \begin{pmatrix} 0 & 0 \\ 0 & q_{--} \end{pmatrix}, \quad \tilde{l}_{+-}^d = \begin{pmatrix} 0 & q_{+-} \\ 0 & 0 \end{pmatrix}, \quad \tilde{l}_{-+}^d = \begin{pmatrix} 0 & 0 \\ q_{-+} & 0 \end{pmatrix}. \quad (\text{S14})$$

Again, $q_{++} = q_{--} = \mathbb{I}$; we shall now probe the structure of the off-diagonal matrix q_{+-} .

In this basis, the four *right* eigenoperators r of $\mathcal{L}_0 + \mathcal{L}'$ with zero eigenvalue are just a single diagonal matrix z in each of the four symmetry quadrants in the thermodynamic limit (see Sec. 2). This matrix z is not pure, and in principle has infinite rank although its eigenvalues fall off exponentially quickly as a function of the index, i.e. $z_{jj} \sim e^{-cj}$ for some $c > 0$. In the case of a noiseless subsystem with full rank z , Ref. [S8] proved that the corresponding conserved quantity must be the identity in each symmetry sector for a finite-dimensional Hilbert space. Since our bosonic model has an infinite-dimensional Hilbert space, these results do not immediately apply. Nevertheless, we numerically show that the conserved quantities approach the identity in the thermodynamic limit.

In Fig. S7, we plot the elements of a 10×10 block of the matrix q_{+-} for the case of non-zero dephasing. Indeed, we find that the matrix tends to the identity as we approach the thermodynamic limit. The matrix q_{+-} acquires off-diagonal terms at entries where the corresponding matrix elements z'_{jj} are small, i.e. we are limited by numerical precision. Analogous behavior is observed for the case of non-zero ω , depicted in Fig. S8. So indeed we expect $\lim_{N \rightarrow \infty} q_{+-} = \mathbb{I}$ for the full rank noiseless subsystem. This explains why ρ_i does not lose coherences when relaxing into the steady state of $\mathcal{L}_0 + \mathcal{L}'$.

5. PASSIVE PROTECTION OF A CLASSICAL BIT IN THE WEAK-BROKEN PHASE

Up to now, we have focused on describing the quantum error correcting properties for a qubit encoded in the steady state of \mathcal{L}_0 subject to errors that keep it in the *strong-broken* phase. Here, we show that a classical bit encoded into the steady state of \mathcal{L}_0 will be passively protected against any error which keeps the model in the *weak-broken* phase. This region of parameter space includes single-photon loss, which is non-negligible in experimental setups and represents the dominant decoherence mechanism for photonic cat qubits.

We consider the same protocol as in the main text, but with a restricted initial state: Initialize the system in the state $\rho_i = c|\alpha\rangle\langle\alpha| + (1-c)|-\alpha\rangle\langle-\alpha|$ where $c = 0$ or 1 , which represents the classical bit and satisfies $\mathcal{L}_0(\rho_i) = 0$. (Any choice of $c \in [0, 1]$ will also exhibit protection.) Then quench the state with an “error” for an arbitrary time τ_q to obtain $\rho_m = \exp[(\mathcal{L}_0 + \mathcal{L}')\tau_q](\rho_i)$. Finally, turn off the error and evolve the system with \mathcal{L}_0 for a long time such

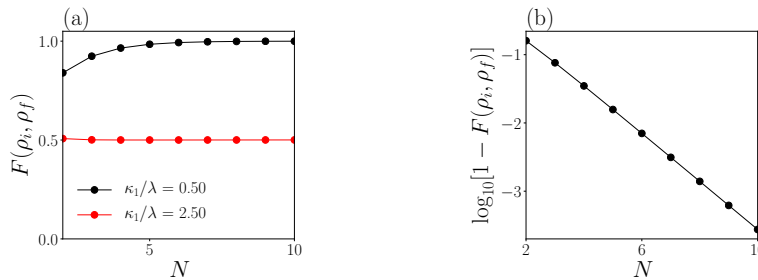


FIG. S9. Fidelity of the initial and final *classical*-bit state with $c = 1, \lambda/\kappa_2 = N, \kappa_d = \omega = 0, \tau_q \lambda = 10, F(\rho_i, \rho_f) = \text{Tr}[\sqrt{\sqrt{\rho_i} \rho_f \sqrt{\rho_i}}]^2$. Quenches to the weak-broken phase (black dots) have a fidelity that tends to one in the thermodynamic limit, while quenches to the weak-unbroken phase (red dots) do not. (b) Same parameters as in (a) with $\kappa_1/\lambda = 0.5$; the fidelity tends to one exponentially fast in N .

that it reaches its steady state: $\rho_f = \lim_{t \rightarrow \infty} \exp[\mathcal{L}_0 t](\rho_m)$. We show that any error which keeps the model in the *weak-broken* phase is correctable passively.

In Fig. S9, we plot the fidelity between the initial and final states after a long quench of single-photon-loss error $L'_1 = \sqrt{\kappa_1} a$. Only if the error keeps the model in the weak-broken phase (i.e. $\kappa_1/\lambda < 2$) does the classical bit recover its initial state in the thermodynamic limit.

We can understand this behavior by considering the steady-state structure for a generic system in the weak-broken phase. In a parity basis, it assumes the form

$$\rho_{ss} = \begin{pmatrix} 1/2 & c - 1/2 \\ c - 1/2 & 1/2 \end{pmatrix} \otimes z, \quad (\text{S15})$$

where $c \in [0, 1]$ is a real variable parameterizing the classical-bit manifold, and z is some (generically mixed) state. This structure is in agreement with Table 2 in the main text. This suggests that any time after the introduction of the error, the state has the form

$$\rho_m(\tau_q) = \begin{pmatrix} 1/2 & c - 1/2 \\ c - 1/2 & 1/2 \end{pmatrix} \otimes M(\tau_q), \quad (\text{S16})$$

where the classical bit c remain perfectly stored in the off-diagonal sector and only M changes. If the error is large enough to move the system to the weak-unbroken phase (e.g. $\kappa_1/\lambda > 2$), then the state will evolve toward a unique steady state and the classical information will be lost. This agrees with our numerical results.

Going back to cat qubit superpositions encoded in the steady state of \mathcal{L}_0 , i.e., $|\psi\rangle = c_1|\alpha\rangle + c_0|-\alpha\rangle$, our analysis implies that “small” single-photon loss ($\kappa_1/\lambda < 2$) can induce phase-flip errors (in the basis above) that are not passively correctable (while keeping bit-flip errors passively correctable), while large single-photon loss ($\kappa_1/\lambda > 2$) can induce both phase-flip and bit-flip errors that are not passively correctable. Errors that cannot be corrected passively must be actively corrected, e.g. via redundantly encoding into ancilla qubits.

-
- [S1] T. Prosen, *New Journal of Physics* **10**, 043026 (2008).
[S2] T. Prosen and T. H. Seligman, *Journal of Physics A: Mathematical and Theoretical* **43**, 392004 (2010).
[S3] V. V. Albert and L. Jiang, *Phys. Rev. A* **89**, 022118 (2014).
[S4] E. Knill, R. Laflamme, and L. Viola, *Phys. Rev. Lett.* **84**, 2525 (2000).
[S5] D. A. Lidar, I. L. Chuang, and K. B. Whaley, *Phys. Rev. Lett.* **81**, 2594 (1998).
[S6] V. V. Albert, B. Bradlyn, M. Fraas, and L. Jiang, *Phys. Rev. X* **6**, 041031 (2016).
[S7] M. Mirrahimi, Z. Leghtas, V. V. Albert, S. Touzard, R. J. Schoelkopf, L. Jiang, and M. H. Devoret, *New Journal of Physics* **16**, 045014 (2014).
[S8] R. Blume-Kohout, H. K. Ng, D. Poulin, and L. Viola, *Phys. Rev. A* **82**, 062306 (2010).